

Contrastive Learning MRI Reconstruction

Mevan Ekanayake^{1,2}, Zhifeng Chen^{1,3}, Gary Egan^{1,4}, Mehrtash Harandi², and Zhaolin Chen^{1,3}

¹Monash Biomedical Imaging, Monash University, Australia

²Department of Electrical and Computer Systems Engineering, Monash University, Australia

³Department of Data Science and AI, Monash University, Australia

⁴School of Psychological Sciences, Monash University, Australia

Corresponding to:

Mevan Ekanayake

Monash Biomedical Imaging

Monash University

Clayton 3168, Victoria, Australia

T: +61 4 3191 9399

E: mevan.ekanayake@monash.edu

Word Count: 4,860

Number of figures: 9

Number of tables: 1

Abstract

Purpose: We propose a novel contrastive learning latent space representation for MRI datasets with partially acquired scans. We show that this latent space can be utilized for accelerated MR image reconstruction.

Theory and Methods: Our novel framework, referred to as COLADA (stands for Contrastive Learning for highly accelerated MR image reconstruction), maximizes the mutual information between differently accelerated images of an MRI scan by using self-supervised contrastive learning. In other words, it attempts to “pull” the latent representations of the same scan together and “push” the latent representations of other scans away. The generated MRI latent space is subsequently utilized for MR image reconstruction and the performance was assessed in comparison to several baseline deep learning reconstruction methods. Furthermore, the quality of the proposed latent space representation was analyzed using Alignment and Uniformity.

Results: COLADA comprehensively outperformed other reconstruction methods with robustness to variations in undersampling patterns, pathological abnormalities, and noise in k-space during inference. COLADA proved the high quality of reconstruction on unseen data with minimal fine-tuning. The analysis of representation quality suggests that the contrastive features produced by COLADA are optimally distributed in latent space.

Conclusion: To the best of our knowledge, this is the first attempt to utilize contrastive learning on differently accelerated images for MR image reconstruction. The proposed latent space representation has practical usage due to a large number of existing partially sampled datasets. This implies the possibility of exploring self-supervised contrastive learning further to enhance the latent space of MRI for image reconstruction.

Keywords: MRI latent space, mutual information maximization, contrastive learning, MR image reconstruction, deep learning

1 Introduction

A major problem in MRI is the extended duration required to acquire data, resulting in discomfort for patients, image artifacts, and elevated examination costs [1]. The study of accelerated MR image reconstruction involves the development and implementation of techniques that enable faster acquisition of MRI data and reconstruction of high-quality images from undersampled data. Deep Learning (DL) has made significant improvements in accelerated MR image reconstruction methods and has been shown to outperform conventional techniques such as compressed sensing and parallel imaging [2]–[6]. DL attempts to solve the image reconstruction problem by learning the parameters of a nonlinear multi-layered model from a large cohort of training data [7]. The architectures of these models often consist of fully-connected networks (FCNs), convolutional neural networks (CNNs), or more recently, vision transformer networks (ViTs) [8]. Regardless of the architectural composition, DL methods for MR image reconstruction can be categorized under two main groups [9]: end-to-end data-driven DL methods that map low-quality undersampled images to high-quality references [10]–[12], and physics-constrained DL methods that iteratively solve the inverse problem of reconstruction [13], [14].

Training of a DL model for MR image reconstruction generally involves tuning the model parameters using paired input-output data to accurately reconstruct high-quality MR images from undersampled k-space data. Like any other time series or high-dimensional modality, the image quality in MRI demonstrates a gradual dependence on the abundance of the acquired signal measurements. For example, the exclusion of a few lines in k-space may not result in an appreciable change in the reconstructed image or a drastic loss of image quality. However, as more and more k-space lines are excluded in order to achieve higher accelerations (8X or 10X), the information content in k-space reduces and results in the reconstruction algorithm failing. This phenomenon was observed in DL models during the second FastMRI challenge in 2020 where radiologists reported that none of the 8X reconstructions submitted were considered clinically acceptable [15]. Likewise, a recent comprehensive review on DL MR image reconstruction pointed out that the existing DL methods show encouraging results only below acceleration factors of 6X [9].

The challenge faced by conventional DL modeling in predicting high-dimensional data, such as MR images, lies not only in the computational intensity of pixel-level loss functions but also in the suboptimal utilization of the model's capacity for learning the predictive distributions of outputs from inputs [16]. For instance, the input MR image to the reconstruction algorithm may contain thousands of bits of information whereas only a portion of them may be essentially useful for accurate reconstruction of an output image with diagnostic quality. Hence, it is important to maximally preserve the information in the input that is most useful in obtaining the desired output. Contrastive learning is a self-supervised DL technique which attempts to maximize the mutual information between learned representations of different views of the input, thereby extracting more useful latent features for a given downstream task [16]. Contrastive learning is widely used in computer vision and has proven to perform well in a range of tasks including image classification, depth estimation, and object detection [17]–[20].

We propose a contrastive learning framework for MRI which extracts latent representations in MRI data for improved image reconstruction [21]. Our main objective is to maximize the mutual information between differently accelerated images of an MRI scan, and thereby preserve the most useful features for the reconstruction of high-quality MR images under high acceleration factors. Our proposed framework referred to as COLADA (*stands for Contrastive Learning for highly Accelerated MR Image*

Reconstruction) leverages contrastive learning on large amounts of undersampled data which is available in most clinical environments. COLADA not only maximizes the scan-specific mutual information between different accelerations of the same scan but also distinguishes undesired features from other scans in the training dataset, measured by Alignment and Uniformity criteria. We have further performed reconstruction and analysis to demonstrate the effectiveness of the contrastive learning latent space representation for MRI.

2 Theory

In this section, we provide the theory of the COLADA framework which produces the contrastive learning representations of MR images.

2.1 Mutual Information Maximization in MRI

We define a set of collected k-space data, $Y \in \mathbb{C}^{M \times N}$, where M is the size of the k-space and N is the total number of scans or k-spaces. We can further randomly undersample y with different acceleration factors to obtain $Y_u \in \mathbb{C}^{M \times D \times N}$ where D is the total number of undersampled k-spaces obtained from each original k-space, e.g., undersampling each k-space using acceleration factors 4X, 6X, and 8X makes $D = 3$. Here Y_u is zero-filled to retain the k-space size M . Note that the original Y can be already undersampled k-spaces. We denote $X_u \in \mathbb{C}^{M \times D \times N}$ as the corresponding image domain data where $X_u = F^H(Y_u)$, and $F^H(\cdot)$ is the inverse Fourier transform operating on the k-space dimension. Thus X_u contains DN number of undersampled MR images and for a given image $x_u = X_u(:, d, n) \in \mathbb{C}^M$, a latent representation can be obtained using $z = T_\phi(x_u)$, where T_ϕ is a DL feature extraction network parametrized by ϕ .

Then we consider a pair of two distinct images (x_u, x'_u) sampled from X_u , i.e. $x_u = X_u(:, d, n) \in \mathbb{C}^M$ and $x'_u = X_u(:, d', n') \in \mathbb{C}^M$. We define (x_u, x'_u) as a positive pair if they originated from the same k-space, i.e., $n = n'$ and we define (x_u, x'_u) as a negative pair if they originated from different k-spaces, i.e. $n \neq n'$. For simplicity, we use (x_u, x_u^+) and (x_u, x_u^-) to denote positive and negative image pairs, respectively. We assume that the positive and negative images maintain their relationship in latent space, hence we use (z, z^+) and (z, z^-) to denote positive and negative latent representation pairs, respectively where $z^+ = T_\phi(x_u^+)$ and $z^- = T_\phi(x_u^-)$. Our objective is to optimize a latent space that maximizes the mutual information between positive pairs as below:

$$\phi^* = \underset{\phi}{\operatorname{argmax}} I(Z, Z^+) \quad (1)$$

where $I(Z, Z^+)$ is the mutual information between the random variables Z, Z^+ that represents the positive latent representation pairs and can be expressed as below:

$$I(Z; Z^+) = \int_z \int_{z^+} P_{(Z, Z^+)}(z, z^+) \log \left(\frac{P_{(Z, Z^+)}(z, z^+)}{P_Z(z)P_{Z^+}(z^+)} \right) dz dz^+ \quad (2)$$

where $P_{Z, Z^+}(z, z^+)$ is the joint probability distribution of Z and Z^+ . By computing the mutual information between two variables, we can gain insights into how much information one variable can

infer from the other, and vice versa. This is a powerful tool in data representation to identify an optimal representation for a given downstream task. The underlying motivation behind this formulation is to extract the mutual information across all latent representations thereby preserving the information content that is relevant to a specific scan. For instance, if we consider two accelerated images, 4X and 10X, of the same scan, we intend to preserve the information of 10X that relates to 4X and vice versa, thereby the information that is not relevant between the pair (which is noise, artifacts, hallucinations, etc.) will be suppressed in the latent space.

2.2 Contrastive Learning Representations in MRI

In practice, it is difficult to compute mutual information directly as it requires estimation of the joint distribution of the two variables with high dimensionality [22]. In this work, we use contrastive learning to maximize mutual information, thereby optimizing the MRI latent space for optimal reconstruction.

Contrastive learning stems from Noise Contrastive Estimation and is often used in computer vision tasks where it is feasible to generate out-of-distribution or noisy data for training. Van den Oord et al. [16] introduced the infoNCE loss to estimate the in-distribution data (or positive pairs) amongst the out-of-distribution (or negative pairs). Motivated by their work [16], [17], we utilized the infoNCE loss as a proxy for our original objective in Eq. 1. During training, for a given minibatch of N k-space acquisitions, for each k-space we generate R undersampled k-spaces using different acceleration factors which total up to NR k-spaces, thereby NR differently undersampled MR images. Thus, for a given undersampled MR image in the minibatch, we have $R - 1$ positive images and we treat the rest of the other $R(N - 1)$ as negative images. Considering each positive pair of images in the minibatch, we define the contrastive learning objective function as follows:

$$L = -\mathbb{E}_{z, z^+} \left[\log \frac{\exp(\text{sim}(z, z^+)/\tau)}{\exp(\text{sim}(z, z^+)/\tau) + \sum_{k=1}^{R(N-1)} \exp(\text{sim}(z, z_k^-)/\tau)} \right] \quad (3)$$

Where $\text{sim}(u, v) = u^T v / \|u\| \|v\|$ (i.e., cosine similarity), and τ is a temperature scaling factor. Minimizing a loss function in Eq. 3 will maximize a lower bound on mutual information [16]. Upon close observation, the loss function in Eq. 3 can also be identified as a conventional log loss (or cross-entropy loss), by which the model is enforced to generate representations that are similar (high cosine similarity) for positive pairs and dissimilar (low cosine similarity) for negative pairs in latent space [23].

To intuitively understand the loss in Eq. 3 in terms of MRI, we consider a set of undersampled images obtained from a particular scan by undersampling the MRI scan by a range of acceleration factors. We can observe common anatomical features which are clearly identifiable at lower acceleration factors but barely identifiable at higher accelerations due to information loss. Now consider another set of undersampled images obtained from a different scan by undersampling the respective MRI scan by a range of acceleration factors and compare it with the images of the first scan. The corresponding MR images belonging to the two scans are distinguishable at lower accelerations but difficult to distinguish at higher accelerations due to the image features arising from aliasing, noise, blurring, etc. Therefore, our goal was to derive a latent space that ‘pulls’ the representations of the same scan together and ‘pushes’ the undesired information away (see Fig. 1). This is done in contrastive learning by placing

the positive pairs in the numerator and the negative pairs in the denominator as in Eq. 3. We propose that a latent space with such a transformation can facilitate subsequent image reconstruction tasks, especially for highly accelerated k-space data.

2.3 Alignment and Uniformity of Contrastive Learning features

To further investigate the effectiveness of the contrastive learning representations, we evaluate their quality in terms of two characteristics, i.e. alignment and uniformity [24]. Alignment evaluates the proximity of features obtained from positive pairs, and uniformity evaluates the consistency of the resultant distribution of features on the hypersphere. It was demonstrated in [24] that improved alignment and uniformity results in improved efficiency in signal representation thereby benefiting subsequent computer vision tasks such as classification and depth estimation.

In the context of MRI, the latent representations extract the most common information between positive pairs and remain invariant to other noise factors such as aliasing artifacts, noise, blurring, etc. In the context of the proposed framework, alignment refers to the closeness or similarity of the contrastive learning features in the latent space learned from differently accelerated images of the same scan and is defined on positive feature pairs using the ℓ_2 distance as below:

$$C_A \triangleq \mathbb{E}_{z, z^+} [\|z - z^+\|_2^\alpha], \quad \alpha > 0 \quad (4)$$

Where α is a controllable parameter which was set to 1 in our evaluations. Uniformity measures how well the contrastive learning features are distributed in the latent space which is an indication of better generalization on downstream tasks and is defined using the Gaussian potential on all feature pairs as below:

$$C_U \triangleq \log \mathbb{E}_{z_i, z_j} \left[\exp \left(-\beta \|z_i - z_j\|_2^\beta \right) \right], \quad \beta > 0 \quad (5)$$

where β is a controllable parameter which was set to 2 in our evaluations. In our experiments, we show that the proposed contrastive learning framework promotes these metrics and produces MR features that are more suitable for image reconstruction.

2.4 Number of positive and negative pairs

In this work, we demonstrated a random undersampling mask with acceleration factors of 4X, 6X, 8X, and 10X while retaining a portion of the center frequencies. In theory, more undersampling masks can also be used. In contrastive learning, instead of mutual information directly, we optimized a lower bound on mutual information. The bound became narrower with increasing negative pairs of images [16] utilized for loss computation in Eq. 3. Thus, increasing the number of differently accelerated images generated from a single scan is a natural way of increasing the number of negative images, and thereby improving contrastive feature learning. However, for a given batch size, the maximum number of differently accelerated images that can be generated is limited by the availability of computational resources.

3 Methods

3.1 COLADA Framework for MR Image Reconstruction

In the DL context, MR image reconstruction is formulated as a regression problem where the parameters of a nonlinear multilayered DL model are trained using a large cohort of training data, D_{tr} consisting of pairs of undersampled k-space measurements y_u and fully sampled references x_r . In our proposed COLADA framework, we attempt to learn the reconstruction via the learned contrastive features explained in the previous section. Thus, we first train a contrastive learning feature extractor, T_ϕ via the optimization in Eq. 3. Then we utilized the optimized model, T_{ϕ^*} to generate contrastive features, $z = T_{\phi^*}(F^H y_u)$, and utilize those contrastive features as the input for the reconstruction DL network, G_θ to learn the optimum model parameters, θ^* as below:

$$\theta^* = \underset{\theta}{\operatorname{argmin}} \mathbb{E}_{(x_r, y_u) \sim D_{tr}} [\mathcal{L}(x_r, G_\theta(z))] \quad (6)$$

where, and \mathcal{L} is a reconstruction loss function. Thus, during training, the model learns the optimal nonlinear mapping between z and x_r . During inference, the image reconstruction on an undersampled k-space can be estimated directly by $\hat{x} = G_{\theta^*}(T_{\phi^*}(F^H y_u))$. The overall schematic of the COLADA framework is shown in Fig. 2. Note that during the contrastive learning, a nonlinear head has been incorporated in T_ϕ whereas it is discarded during reconstruction. This strategy has proven to improve feature extraction [17].

3.2 Datasets

For the training and validation of our proposed COLADA framework, the fastMRI brain dataset [1] (<https://fastmri.org/dataset/>) was utilized. The brain dataset consists of fully sampled complex-valued k-space data obtained on 3 and 1.5 Tesla magnets and includes axial T1-weighted, T2-weighted, and FLAIR scans with some of the T1-weighted acquisitions including admissions of contrast agent (T1-POST). The number of MR volumes and 2D slices utilized during contrastive feature extraction and image reconstruction are given in Table 1. All models (COLADA and other comparative methods) were trained on FLAIR, T1, T2, and T1-POST scans together. The intensity values of the brain images were scaled in the range [0,1] for better convergence in DL training.

3.3 Implementation

The COLADA framework was trained on an NVIDIA A40 GPU for 100 epochs in a batch size of 8 using an RMSProp optimizer with a learning rate of 0.0001. The contrastive learning feature extractor was implemented in U-Net architecture [25] and a D5C5 [26] was implemented as the reconstruction backbone network. Literature on Contrastive learning suggests the usage of a nonlinear head during training for improved results, hence we implemented an MLP-Mixer [27] as the non-linear head which was discarded during inference. We retrospectively undersampled each scan using acceleration factors 4X, 6X, 8X, and 10X using random masks. To train the contrastive learning feature extractor, we utilized the loss as in Eq. 3. with a batch size of 64 (3 positive samples and 60 negative samples for each image), and for the reconstruction, we utilized the ℓ_1 -norm loss with a batch size of 8. The convergence of the model training is discussed in Appendix A.1.

3.4 Experiments

The reconstruction performance of COLADA was assessed both quantitatively and qualitatively. Our experiments evaluated the effectiveness and robustness of the method under different adversarial conditions. We compared the performance of the COLADA method with that of two other standard reconstruction models, i.e. U-Net [1] which performs image-to-image mapping, and a D5C5 [26] network which is a cascaded reconstruction model with data consistency in k-space. Both these models were implemented using image data for input and supervised learning for training. Additionally, the experiments included an assessment of the quality of representations generated by COLADA in terms of Alignment and Uniformity in the hypersphere in comparison to random initialization and supervised learning.

3.4.1 Evaluation of Reconstruction Performance

In order to assess the efficacy of the COLADA method in accelerated MR image reconstruction using undersampling k-space, we compared the reconstruction performance qualitatively as well as quantitatively using Normalized Mean Square Error (NMSE), Peak Signal to Noise ratio (PSNR), and Structural Similarity Index (SSIM). During inference, a random undersampling mask was used with a portion of the central k-space always sampled following standard practice [1]. We tested not only the accelerations that the models were trained on (4X and 10X) but also a case with high acceleration (16X).

While DL models are typically trained on specific k-space undersampling patterns, they may differ in practical situations due to changes in the imaging field of view. Hence, the undersampling pattern is an important aspect of MRI and a comprehensive reconstruction method must be robust to the undersampling pattern in k-space. We examined how changes in the undersampling pattern during inference affect the reconstruction capabilities of COLADA in comparison to other methods by inferring the models on equispaced undersampling. Note that the models were trained on random undersampling.

It is crucial to test DL algorithms on out-of-distribution data such as MR images with tumors, lesions, or other abnormalities, as the training data may not contain sufficient examples of such cases. Evaluation of the performance solely using in-distribution data may lead to overconfident yet erroneous predictions. Thus, we evaluated the performance of the COLADA method using MR images with tumors to assess the out-of-distribution reconstruction performance for images with brain tumors.

To study the generalizability of a reconstruction model, it is important to evaluate the model's performance across diverse data distributions, identify potential biases and limitations, enhance the model's robustness, and promote advances for improved clinical application. We assessed the performance of COLADA on a locally acquired dataset consisting of 25 T1-weighted scans [28] and did not retrain or finetune the contrastive learning feature extractor for the new dataset, although we did fine-tune the downstream reconstruction model for a single epoch to obtain optimum results.

MR images display varying signal-to-noise (SNR) properties based on imaging parameters including TE/TR/flip-angle/image resolution [29]. To investigate the impact of SNR variations on reconstruction, we introduced additive white Gaussian noise (AWGN) of 30dB, 20dB, and 10dB to the undersampled complex-valued k-space data and evaluated the effect on the reconstructed image using COLADA and other methods.

3.4.2 Analysis of Quality of Latent Representation

We assessed the representation quality of COLADA in terms of two properties, Alignment and Uniformity in the hypersphere in order to understand how the contrastive learning features possess unique characteristics for image reconstruction. For the Alignment analysis, we show histograms of ℓ_2 distances between features of positive pairs and observed the proximity between each acceleration factor pair separately.

For the Uniformity analysis, we modified the Feature Extractor used for contrastive learning to output a two-dimensional feature vector, i.e., the extracted contrastive learning features lie on a unit circle. We plotted the distributions of features with Gaussian kernel density estimation (KDE) on the unit circle to visualize the spread of the features from the validation set. In both analyses, we compared the corresponding results with a randomly initialized feature extractor as well as a supervised trained feature extractor with the same neural network architecture for a fair comparison.

4 Results

Fig. 3 shows the reconstructed images using different methods at acceleration factors of 4X, 10X, and 16X for two different contrasts, T1 and FLAIR. Visual inspection showed COLADA achieves high reconstruction quality even at very higher acceleration factors. Further qualitative analysis can be found in Appendix A.2. Fig. 4 demonstrates the quantitative boxplot scores for the validation dataset with respect to NMSE, PSNR, and SSIM. It is evident that all three metrics reflect superior scores compared with U-Net and D5C5. The numerical score values are presented in Appendix A.3.

Fig. 5 demonstrates inference on 8X undersampled k-space using an equispaced sampling pattern. It is noteworthy that the DL models have been trained on random undersampling. Here, D5C5 produces low-quality images in all contrasts with residual aliasing artifacts on a global scale. U-Net is able to reconstruct the images quite accurately with minimum error nevertheless contains blurring. However, COLADA is comparatively accurate with a small error and high-image quality.

In Fig. 6, we test 6X reconstructions on images of different contrasts which also consist of a tumor. These types of pathological abnormalities are highly underrepresented in the training dataset and can thus create greater uncertainty in reconstruction [30]. COLADA achieves greater capabilities of accurately reconstructing the tumor region with commendable contrast. Here, U-Net reconstructions are comparatively blurry resulting in difficulty to clearly identify the tumor. D5C5 reconstructions show better contrast in the tumor regions compared to U-Net, however, the overall image has residual artifacts and poor image quality.

Fig. 7 demonstrates two test cases of T1-weighted image reconstructions from a locally acquired dataset undersampled using accelerations 4X, 6X, 8X, and 10X. Note that the contrastive learning feature extractor was trained on the fastMRI dataset without fine-tuning, while the reconstruction network was only finetuned for a single epoch. It can be seen that the COLADA framework can be adopted for in-vivo reconstructions with minimum finetuning. The reconstruction quality at 10X is commendable when compared with the reference. It is also notable that the reconstructions are less noisy compared to the reference due to the convolutional operations within the COLADA framework. The quantitative scores of this experiment are presented in Appendix A.4.

Fig. 8 demonstrates the reconstructions when AWGN complex-valued noise is present at the acquired k-space of magnitude 30 dB, 20 dB, and 10 dB. Here we used 8X random undersampling. It is seen that U-Net reconstruction contains noise throughout the imaging field of view and drastically blurs out when noise is 10dB. D5C5 reconstruction fails to reconstruct edge features accurately in the presence of noise as is seen from the error maps. In contrast, COLADA reconstructions have a minimum error and the increase in error with noise is not noticeable. We believe that the noise features are suppressed in the contrastive learning MRI latent space which results in robustness to noise.

In our final experiment, we assessed the quality of the extracted MRI representations from COLADA in terms of alignment and uniformity. Observing the left column of Fig. 9, it can be seen that the contrastive learning MRI representations of the positive pairs lie close to each other in the latent space with an average alignment score of $C_A = 0.0996$ whereas the MRI representations of positive pairs from random initialization and supervised learning lie comparatively distantly with alignment scores of $C_A = 0.8776$ and $C_A = 0.7646$, respectively. Upon closer observation of the distance distribution of the MRI representations of positive pairs, it is evident that the distances between numerically close accelerations such as 4X-6X, 6X-8X, and 8X-10X are lower and biased towards the left side of the distribution whereas the distances between numerically apart accelerations such as 4X-8X, 4X-10X, and 6X-10X are higher and biased towards to the right side of the distribution. This shows that contrastive learning enforces alignment of the numerically closer accelerations in MRI latent space, but finds it comparatively harder to align the accelerations that are numerically apart. However, all accelerations pairs show lower distances compared to the random initialization and supervised learning cases.

Fig. 9 also demonstrates the superior uniformity of the contrastive learning MRI latent space on the unit circles compared to random initialization and supervised learning. The features are shown in two-dimensional vectors separately for the four contrasts in the validation set, T1, T2, T1-POST, and FLAIR. In order to understand the distribution properly, a Kernel Density Estimation (KDE) has been carried out and it is clear that the contrastive learning results in distributions that are more uniform across the latent space compared to random initialization or supervised learning. In the random initialization case, the features are clustered to a singular region of the latent space whereas in the supervised learning case, the features are clustered to several locations only. Conversely, the features from COLADA are uniformly distributed throughout the latent space which the authors of [24] identify as a favorable quality of representations for downstream tasks.

5 Discussion

The proposed COLADA framework shows promising results in MR image reconstruction under high acceleration factors. By maximizing the mutual information between differently accelerated images of MRI scans, COLADA is able to preserve the most useful features in latent space. This is achieved through a two-phase process, where first, a DL feature extractor is pre-trained using contrastive learning, and in the second phase, the pre-trained model is utilized to generate contrastive learning MRI representations on which the reconstruction model is trained to produce high-quality MR images. Unlike conventional supervised DL techniques, COLADA constitutes an MRI feature extraction procedure which is self-supervised and convenient in the clinical setting, where undersampled MRI

measurements are available without the fully sampled acquisitions. It is also applicable in the fully sampled setting by applying retrospective undersampling.

When inferred on images from the same dataset that the models were trained on, COLADA depicted superior performance over the other methods qualitatively as well as quantitatively. Further experiments demonstrated the robustness of COLADA to the variations in the undersampling pattern and to images containing tumors. Also, it was seen that the proposed framework could be readily applied to in-vivo scanning upon a small amount of fine-tuning with limited data. The experiments involving noise injection to k-space showed that the contrastive learning latent space is capable of suppressing noise as a result of maximizing the most important information. Further assessment of the quality of contrastive learning MRI features in terms of alignment and uniformity showed that the positive pairs were well-aligned, and the overall features were uniformly distributed across the MRI latent space compared to random initialization and supervised learning.

One potential limitation of the proposed framework is that it requires a large cohort of undersampled MRI measurements for contrastive learning including multiple differently accelerated images of the same scan. However, this may not be feasible in certain clinical settings where large cohorts of undersampled acquisitions may not be available. Also, the performance of contrastive learning highly depends on the number of negative samples utilized for optimization in Eq. 3, which is limited by computational resources. Thus, to yield the maximum advantage of contrastive learning, access to large GPU memory is required which may not be feasible in many cases.

Another main limitation of the current work is that it functions in the single-coil setting whereas MRI scanners generally acquire multi-coil MRI data. However, the framework could be adapted for the multi-coil setting by manipulating the number of input/output channels of the DL models, and the coil sensitivities incorporated following a procedure similar to [31].

We acknowledge that limited analysis has been carried out in terms of design choices and hyperparameter tuning of the DL models in COLADA. We believe many factors like the number of accelerations utilized for contrastive learning, the range of accelerations utilized for contrastive learning, the size of the latent space, the optimal utilization of contrastive latent features for reconstruction (e.g., fusion techniques between image and contrastive learning features) and many more factors could affect the contrastive learning process.

It is noteworthy that the COLADA method can be used when fully-sampled acquisitions are not available. For instance, given a dataset with 2X acquisitions, it is possible to retrospectively undersample further to obtain higher accelerations such as 4X, 6X, etc., and by designing suitable masks it is possible to generate even more continuously varying accelerations such as 2.1X, and 2.2X. Another option would be to vary the sampling pattern in k-space to generate images from a single MRI scan and our results show robustness to different sampling patterns. Motivated by DL, another suitable choice would be to add a layer of trainable parameters on top of the sampling operator such that the model itself will learn a suitable set of undersampling rules that maximize the mutual information between positive features.

The intuition behind COLADA is to preserve the most useful features of an MR image in the latent space by considering a range of differently undersampled images of the same scan, hence encoding image information in latent space. However, it is possible to adapt this concept to encode additional

information such as contrast/sequence type, slice location, or other parameters like T1, T2, etc. (e.g., “pull” multiple scans of the same imaging sequence/contrast together while “pull” the scans of other sequences/contrasts away)

In terms of the contrastive learning algorithm, COLADA is fundamentally based on the work of [17], most commonly referred to as SimCLR. However, more recent algorithms such as Moco [32], Swav [33], DINO [19], BYOL [20], and Barlow Twins [34] have shown comparable improvements over SimCLR in various vision tasks. Our future work will also focus on incorporating these novel contrastive learning algorithms.

6 Conclusions

In conclusion, we proposed a novel latent space for MR image reconstruction which can be utilized effectively for high-quality image reconstruction. Our experiments demonstrated the superior performance of our framework, COLADA, over well-established DL MR image reconstruction methods even in the presence of out-of-distribution inputs. Further analysis of representation quality in terms of alignment and uniformity suggested that the MRI features are well distributed in the proposed latent space. COLADA offers a promising solution to the challenges faced by conventional supervised DL modeling as contrastive learning does not require fully-sampled MRI acquisitions for model training.

Acknowledgments

This work was conducted as a part of the projects titled “Simultaneous to synergistic MR-PET: integrative brain imaging technologies” funded by the Australian Research Council Linkage Program (LP170100494) and “Biophysics-informed deep learning framework for magnetic resonance imaging” funded by the Australian Research Council Discovery Program (DP210101863), and Australian Research Council Fellowship Program (IM230100002).

References

- [1] J. Zbontar *et al.*, ‘fastMRI: An Open Dataset and Benchmarks for Accelerated MRI’, *arXiv:1811.08839 [physics, stat]*, Dec. 2019, Accessed: Mar. 20, 2022. [Online]. Available: <http://arxiv.org/abs/1811.08839>
- [2] F. Knoll *et al.*, ‘Deep-Learning Methods for Parallel Magnetic Resonance Imaging Reconstruction: A Survey of the Current Approaches, Trends, and Issues’, *IEEE Signal Processing Magazine*, vol. 37, no. 1, pp. 128–140, Jan. 2020, doi: 10.1109/MSP.2019.2950640.
- [3] C. M. Sandino, J. Y. Cheng, F. Chen, M. Mardani, J. M. Pauly, and S. S. Vasanawala, ‘Compressed Sensing: From Research to Clinical Practice With Deep Neural Networks: Shortening Scan Times for Magnetic Resonance Imaging’, *IEEE Signal Processing Magazine*, vol. 37, no. 1, pp. 117–127, Jan. 2020, doi: 10.1109/MSP.2019.2950433.
- [4] M. Lustig, D. Donoho, and J. M. Pauly, ‘Sparse MRI: The application of compressed sensing for rapid MR imaging’, *Magn. Reson. Med.*, vol. 58, no. 6, pp. 1182–1195, Dec. 2007, doi: 10.1002/mrm.21391.

- [5] K. P. Pruessmann, M. Weiger, M. B. Scheidegger, and P. Boesiger, 'SENSE: Sensitivity encoding for fast MRI', *Magnetic Resonance in Medicine*, vol. 42, no. 5, pp. 952–962, 1999, doi: 10.1002/(SICI)1522-2594(199911)42:5<952::AID-MRM16>3.0.CO;2-S.
- [6] D. K. Sodickson and W. J. Manning, 'Simultaneous acquisition of spatial harmonics (SMASH): Fast imaging with radiofrequency coil arrays', *Magnetic Resonance in Medicine*, vol. 38, no. 4, pp. 591–603, 1997, doi: 10.1002/mrm.1910380414.
- [7] D. Liang, J. Cheng, Z. Ke, and L. Ying, 'Deep Magnetic Resonance Image Reconstruction: Inverse Problems Meet Neural Networks', *IEEE Signal Processing Magazine*, vol. 37, no. 1, pp. 141–151, Jan. 2020, doi: 10.1109/MSP.2019.2950557.
- [8] M. Ekanayake, K. Pawar, M. Harandi, G. Egan, and Z. Chen, 'Multi-branch Cascaded Swin Transformers with Attention to k-space Sampling Pattern for Accelerated MRI Reconstruction'. arXiv, Dec. 21, 2022. doi: 10.48550/arXiv.2207.08412.
- [9] S. Wang, T. Xiao, Q. Liu, and H. Zheng, 'Deep learning for fast MR imaging: A review for learning reconstruction from incomplete k-space data', *Biomedical Signal Processing and Control*, vol. 68, p. 102579, Jul. 2021, doi: 10.1016/j.bspc.2021.102579.
- [10] G. Yang *et al.*, 'DAGAN: Deep De-Aliasing Generative Adversarial Networks for Fast Compressed Sensing MRI Reconstruction', *IEEE Transactions on Medical Imaging*, vol. 37, no. 6, pp. 1310–1321, Jun. 2018, doi: 10.1109/TMI.2017.2785879.
- [11] B. Zhu, J. Z. Liu, S. F. Cauley, B. R. Rosen, and M. S. Rosen, 'Image reconstruction by domain-transform manifold learning', *Nature*, vol. 555, no. 7697, Art. no. 7697, Mar. 2018, doi: 10.1038/nature25988.
- [12] T. Eo, Y. Jun, T. Kim, J. Jang, H.-J. Lee, and D. Hwang, 'KIKI-net: cross-domain convolutional neural networks for reconstructing undersampled magnetic resonance images', *Magnetic Resonance in Medicine*, vol. 80, no. 5, pp. 2188–2201, 2018, doi: 10.1002/mrm.27201.
- [13] yan yang, J. Sun, H. Li, and Z. Xu, 'Deep ADMM-Net for Compressive Sensing MRI', in *Advances in Neural Information Processing Systems*, Curran Associates, Inc., 2016. Accessed: Mar. 20, 2022. [Online]. Available: <https://proceedings.neurips.cc/paper/2016/hash/1679091c5a880faf6fb5e6087eb1b2dc-Abstract.html>
- [14] K. Hammernik *et al.*, 'Learning a variational network for reconstruction of accelerated MRI data', *Magnetic Resonance in Medicine*, vol. 79, no. 6, pp. 3055–3071, 2018, doi: 10.1002/mrm.26977.
- [15] M. J. Muckley *et al.*, 'Results of the 2020 fastMRI Challenge for Machine Learning MR Image Reconstruction', *IEEE Trans. Med. Imaging*, vol. 40, no. 9, pp. 2306–2317, Sep. 2021, doi: 10.1109/TMI.2021.3075856.
- [16] A. van den Oord, Y. Li, and O. Vinyals, 'Representation Learning with Contrastive Predictive Coding'. arXiv, Jan. 22, 2019, doi: 10.48550/arXiv.1807.03748.
- [17] T. Chen, S. Kornblith, M. Norouzi, and G. Hinton, 'A Simple Framework for Contrastive Learning of Visual Representations', in *Proceedings of the 37th International Conference on Machine Learning*, PMLR, Nov. 2020, pp. 1597–1607. Accessed: Sep. 06, 2022. [Online]. Available: <https://proceedings.mlr.press/v119/chen20j.html>
- [18] P. Khosla *et al.*, 'Supervised Contrastive Learning', in *Advances in Neural Information Processing Systems*, Curran Associates, Inc., 2020, pp. 18661–18673. Accessed: Oct. 18, 2022. [Online]. Available: <https://proceedings.neurips.cc/paper/2020/hash/d89a66c7c80a29b1bdbab0f2a1a94af8-Abstract.html>
- [19] M. Caron *et al.*, 'Emerging Properties in Self-Supervised Vision Transformers', in *2021 IEEE/CVF International Conference on Computer Vision (ICCV)*, Montreal, QC, Canada: IEEE, Oct. 2021, pp. 9630–9640. doi: 10.1109/ICCV48922.2021.00951.
- [20] J.-B. Grill *et al.*, 'Bootstrap Your Own Latent - A New Approach to Self-Supervised Learning', in *Advances in Neural Information Processing Systems*, Curran Associates, Inc., 2020, pp. 21271–21284. Accessed: Mar. 28, 2023. [Online]. Available: <https://proceedings.neurips.cc/paper/2020/hash/f3ada80d5c4ee70142b17b8192b2958e-Abstract.html>

- [21] M. Ekanayake, Z. Chen, K. Pawar, G. Egan, M. Harandi, and Z. Chen, ‘COLADA: Contrastive Learning for highly accelerated MR Image Reconstruction’, presented at the 2023 ISMRM & ISMRT Annual Meeting & Exhibition, Toronto, Canada, 2023.
- [22] L. Paninski, ‘Estimation of Entropy and Mutual Information’, *Neural Computation*, vol. 15, no. 6, pp. 1191–1253, Jun. 2003, doi: 10.1162/089976603321780272.
- [23] D. McAllester, ‘Information Theoretic Co-Training’. arXiv, Aug. 14, 2018. doi: 10.48550/arXiv.1802.07572.
- [24] T. Wang and P. Isola, ‘Understanding Contrastive Representation Learning through Alignment and Uniformity on the Hypersphere’, in *Proceedings of the 37th International Conference on Machine Learning*, PMLR, Nov. 2020, pp. 9929–9939. Accessed: Jun. 01, 2023. [Online]. Available: <https://proceedings.mlr.press/v119/wang20k.html>
- [25] O. Ronneberger, P. Fischer, and T. Brox, ‘U-Net: Convolutional Networks for Biomedical Image Segmentation’, in *Medical Image Computing and Computer-Assisted Intervention – MICCAI 2015*, N. Navab, J. Hornegger, W. M. Wells, and A. F. Frangi, Eds., in Lecture Notes in Computer Science, vol. 9351. Cham: Springer International Publishing, 2015, pp. 234–241. doi: 10.1007/978-3-319-24574-4_28.
- [26] J. Schlemper, J. Caballero, J. V. Hajnal, A. Price, and D. Rueckert, ‘A Deep Cascade of Convolutional Neural Networks for MR Image Reconstruction’, in *Information Processing in Medical Imaging*, M. Niethammer, M. Styner, S. Aylward, H. Zhu, I. Oguz, P.-T. Yap, and D. Shen, Eds., in Lecture Notes in Computer Science. Cham: Springer International Publishing, 2017, pp. 647–658. doi: 10.1007/978-3-319-59050-9_51.
- [27] I. O. Tolstikhin *et al.*, ‘MLP-Mixer: An all-MLP Architecture for Vision’, in *Advances in Neural Information Processing Systems*, Curran Associates, Inc., 2021, pp. 24261–24272. Accessed: Nov. 07, 2022. [Online]. Available: <https://proceedings.neurips.cc/paper/2021/hash/cba0a4ee5ccd02fda0fe3f9a3e7b89fe-Abstract.html>
- [28] S. D. Jamadar *et al.*, ‘Simultaneous BOLD-fMRI and constant infusion FDG-PET data of the resting human brain’, *Sci Data*, vol. 7, no. 1, Art. no. 1, Oct. 2020, doi: 10.1038/s41597-020-00699-5.
- [29] Z. Chen, K. Pawar, M. Ekanayake, C. Pain, S. Zhong, and G. F. Egan, ‘Deep Learning for Image Enhancement and Correction in Magnetic Resonance Imaging—State-of-the-Art and Challenges’, *J Digit Imaging*, vol. 36, no. 1, pp. 204–230, Feb. 2023, doi: 10.1007/s10278-022-00721-9.
- [30] M. Ekanayake, K. Pawar, G. Egan, and Z. Chen, ‘PixCUE: Joint Uncertainty Estimation and Image Reconstruction in MRI using Deep Pixel Classification’. arXiv, Mar. 08, 2023. doi: 10.48550/arXiv.2303.00111.
- [31] A. Sriram *et al.*, ‘End-to-End Variational Networks for Accelerated MRI Reconstruction’, in *Medical Image Computing and Computer Assisted Intervention – MICCAI 2020*, A. L. Martel, P. Abolmaesumi, D. Stoyanov, D. Mateus, M. A. Zuluaga, S. K. Zhou, D. Racoceanu, and L. Joskowicz, Eds., in Lecture Notes in Computer Science. Cham: Springer International Publishing, 2020, pp. 64–73. doi: 10.1007/978-3-030-59713-9_7.
- [32] K. He, H. Fan, Y. Wu, S. Xie, and R. Girshick, ‘Momentum Contrast for Unsupervised Visual Representation Learning’, in *2020 IEEE/CVF Conference on Computer Vision and Pattern Recognition (CVPR)*, Seattle, WA, USA: IEEE, Jun. 2020, pp. 9726–9735. doi: 10.1109/CVPR42600.2020.00975.
- [33] M. Caron, I. Misra, J. Mairal, P. Goyal, P. Bojanowski, and A. Joulin, ‘Unsupervised Learning of Visual Features by Contrasting Cluster Assignments’, in *Advances in Neural Information Processing Systems*, Curran Associates, Inc., 2020, pp. 9912–9924. Accessed: May 25, 2023. [Online]. Available: <https://proceedings.neurips.cc/paper/2020/hash/70feb62b69f16e0238f741fab228fec2-Abstract.html>
- [34] J. Zbontar, L. Jing, I. Misra, Y. LeCun, and S. Deny, ‘Barlow Twins: Self-Supervised Learning via Redundancy Reduction’, in *Proceedings of the 38th International Conference on Machine Learning*, PMLR, Jul. 2021, pp. 12310–12320. Accessed: May 25, 2023. [Online]. Available: <https://proceedings.mlr.press/v139/zbontar21a.html>

Tables and Figures

Table 1: Contrast distribution of the number of MRI volumes [2D slices] utilized for training and validation.

Contrast	Contrastive Learning		Reconstruction	
	Training	Validation	Training	Validation
T1	400 [6254]	100 [1552]	100 [1548]	25 [390]
T2	400 [6356]	100 [1598]	100 [1590]	25 [400]
T1-POST	400 [6296]	100 [1580]	100 [1584]	25 [400]
FLAIR	400 [5440]	100 [1582]	100 [1584]	25 [396]

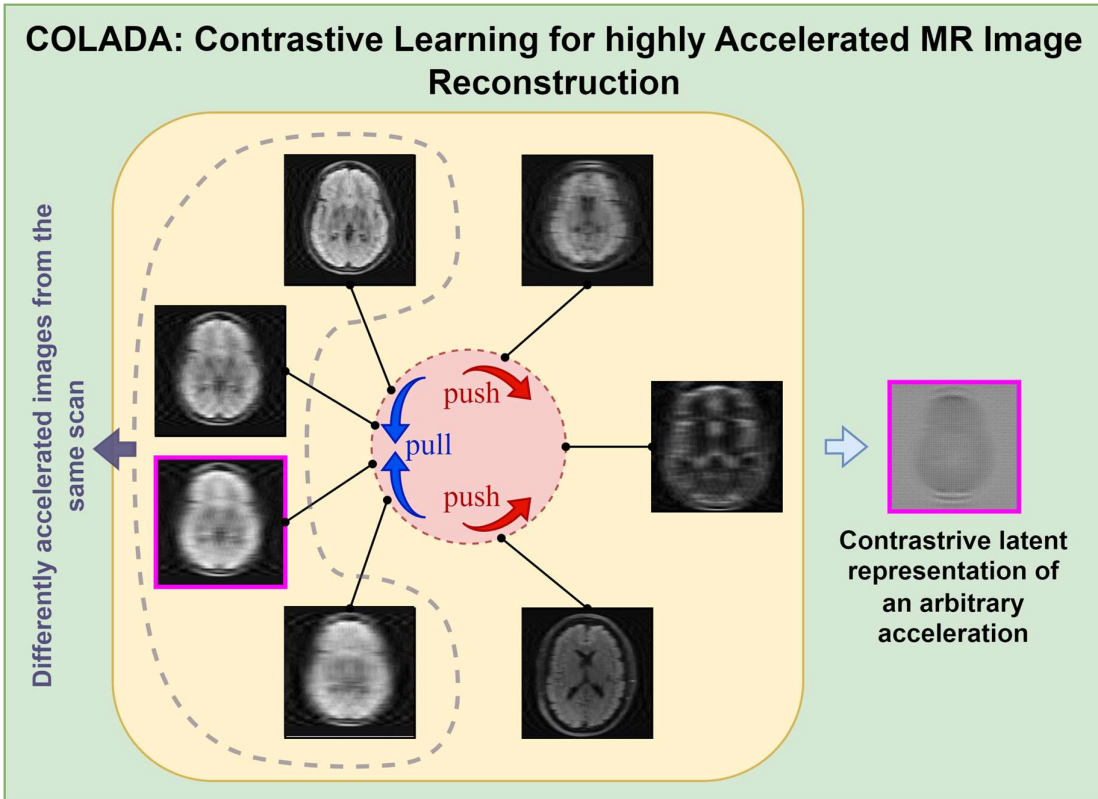


Fig. 1 The underlying concept behind the proposed framework COLADA: Pulling the representations of differently accelerated images of the same scan together while pushing the other scans away in latent space. The resulting latent space representation can be effectively utilized for subsequent reconstruction.

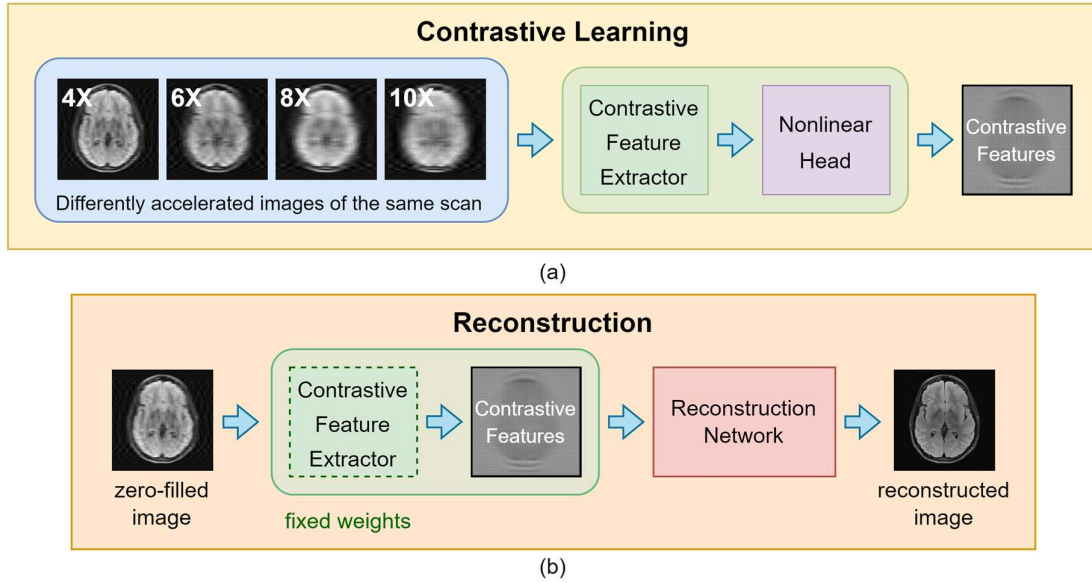


Fig. 2 Overview of the proposed COLADA framework. Contrastive Learning: a range of differently accelerated images are generated for each scan by using a range of accelerations. These images are then used to train a contrastive feature extractor which is utilized to generate contrastive features. Reconstruction: The trained contrastive feature extractor is fixed, and the generated contrastive features are subsequently utilized to train a reconstruction network.

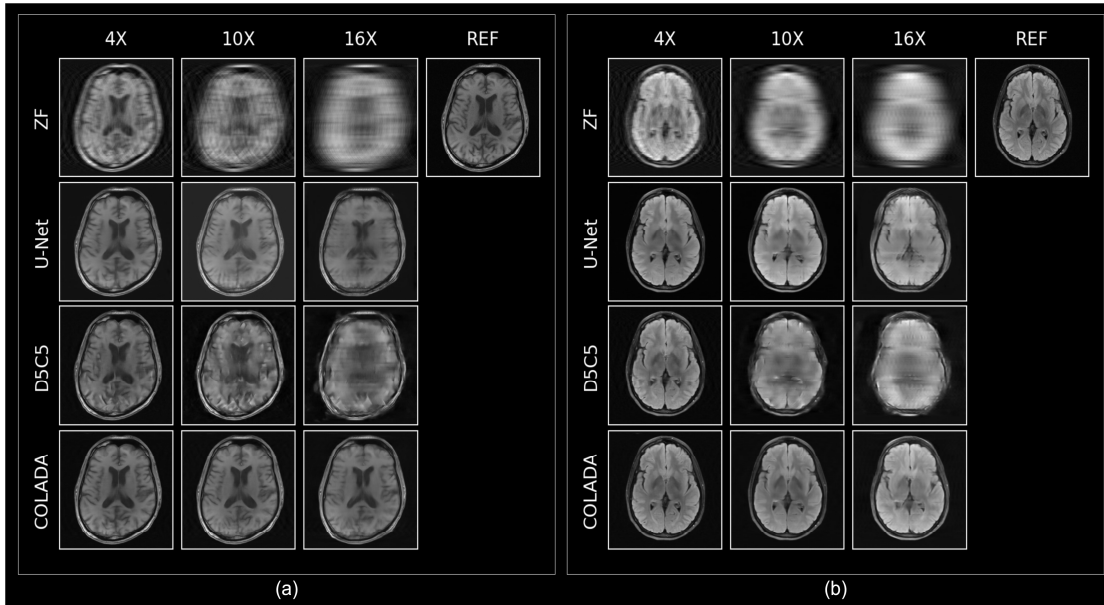


Fig. 3 Qualitative reconstruction comparison of random undersampling in k-space at acceleration factors of 4X, 10X, and 16X for two different contrasts, (a) T1 and (b) FLAIR. ZF: zero-filled input image to DL network reconstructed from undersampled k-space; REF: ground truth fully sampled image; U-Net: reconstructed image using image-to-image mapping DL network. D5C5: reconstructed image using cascaded DL network with data consistency by originally sampled k-space. COLADA: reconstructed image using the COLADA framework. Visual inspection suggests superior reconstruction quality of COLADA even at high acceleration factors.

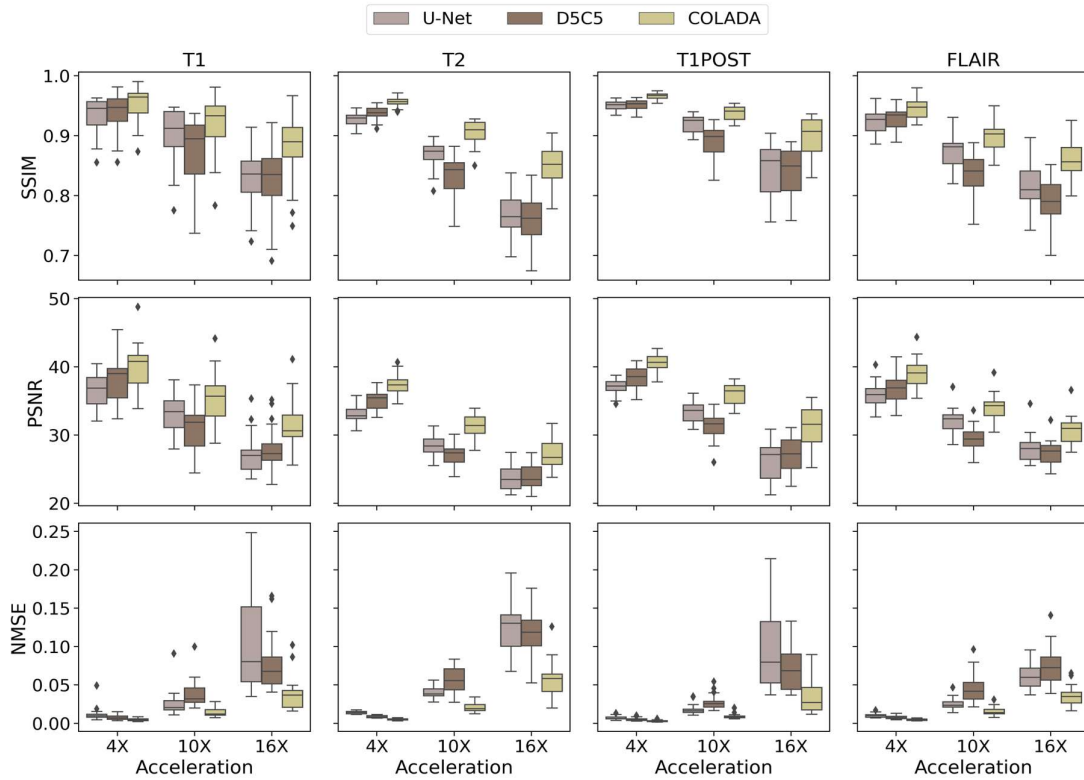


Fig. 4 Quantitative reconstruction comparison of random undersampling in k-space at acceleration factors of 4X, 10X, and 16X with respect to NMSE, PSNR, and SSIM for the four image contrasts (T1, T2, T1POST, and FLAIR) in the validation set. U-Net: reconstructed image using image-to-image mapping DL network. D5C5: reconstructed image using cascaded DL network with data consistency by originally sampled k-space. COLADA: reconstructed image using the COLADA framework. Quantitative scores demonstrate superior reconstruction performance of the COLADA framework.

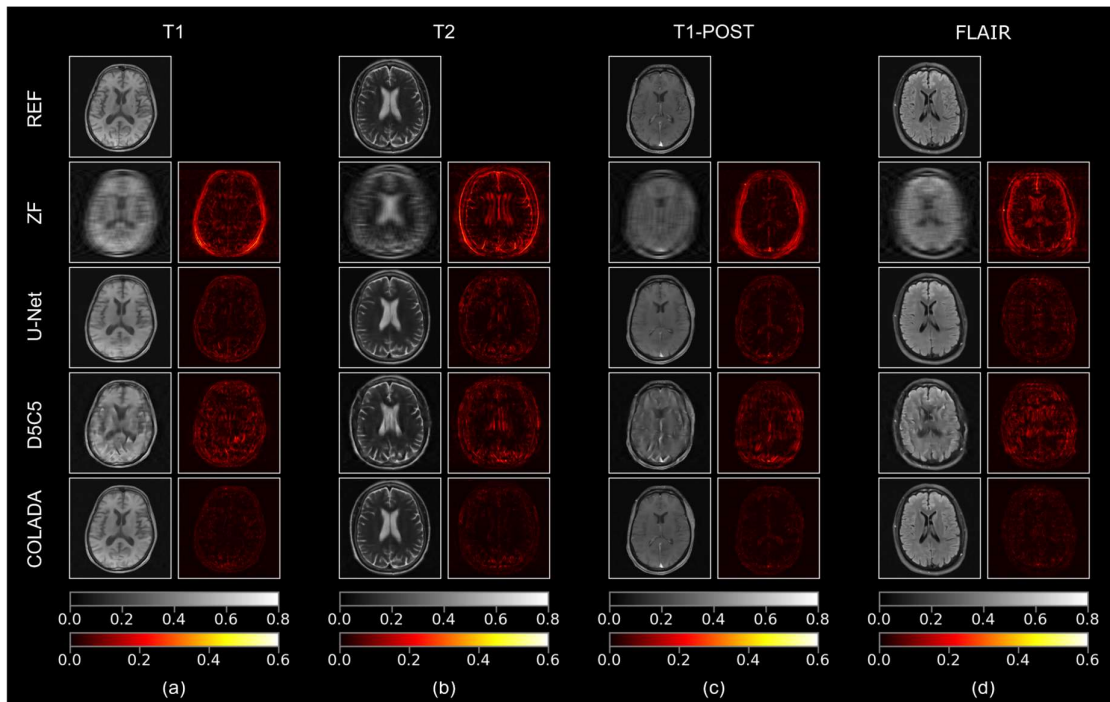


Fig. 5 Qualitative reconstruction comparison of equispaced undersampling in k-space at an acceleration factor of 8X using the models trained on random undersampling. The reconstructions along with the absolute error are shown for (a) T1 (b) T2 (c) T1-POST, and (d) FLAIR scans. ZF: zero-filled input image to DL network reconstructed from undersampled k-space; REF: ground truth fully sampled image; U-Net: reconstructed image using image-to-image mapping DL network. D5C5: reconstructed image using cascaded DL network with data consistency by originally sampled k-space. COLADA: reconstructed image using the COLADA framework. Visual inspections demonstrate the robustness of the COLADA method to the undersampling pattern in k-space.

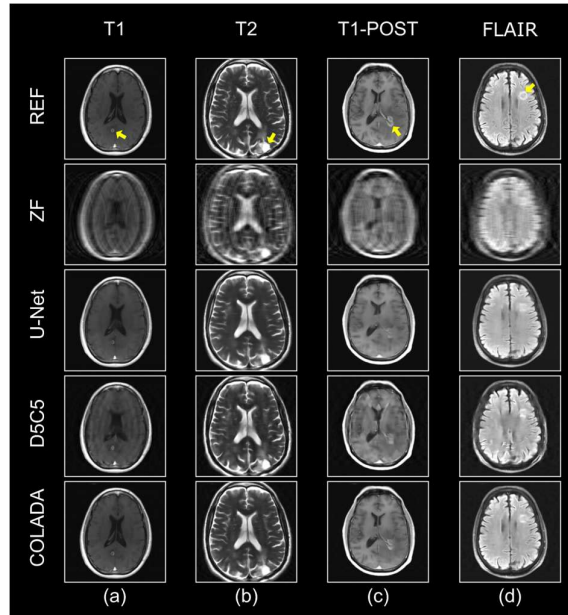


Fig. 6 Qualitative reconstruction comparison of random undersampling in k-space at an acceleration factor of 6X on MR images which contain tumors. The reconstructions along with the region of interest are shown using a yellow arrow for (a) T1 (b) T2 (c) T1-POST, and (d) FLAIR scans. ZF: zero-filled input image to DL network reconstructed from undersampled k-space; REF: ground truth fully sampled image; U-Net: reconstructed image using image-to-image mapping DL network [1]. D5C5: reconstructed image using cascaded DL network with data consistency by originally sampled k-space [22]. COLADA: reconstructed image using the COLADA framework. Visual inspection suggests the superior reconstruction quality of the COLADA method and commendable contrast in the tumor at a high acceleration factor proving the capability of combatting out-of-distribution data.

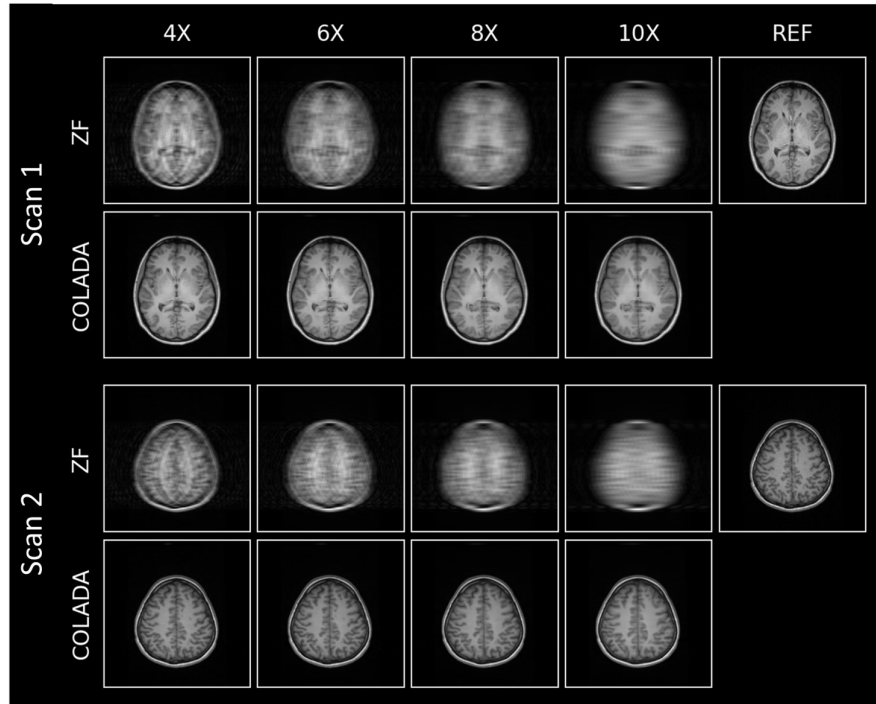


Fig. 7. Inference on two T1-weighted brain scans that were acquired locally. ZF: zero-filled input image to DL network reconstructed from undersampled k-space; REF: ground truth fully sampled image; COLADA: reconstructed image using the COLADA framework. Visual inspection suggests commendable reconstruction quality of COLADA methods and compatibility with external datasets and in-vivo reconstruction.

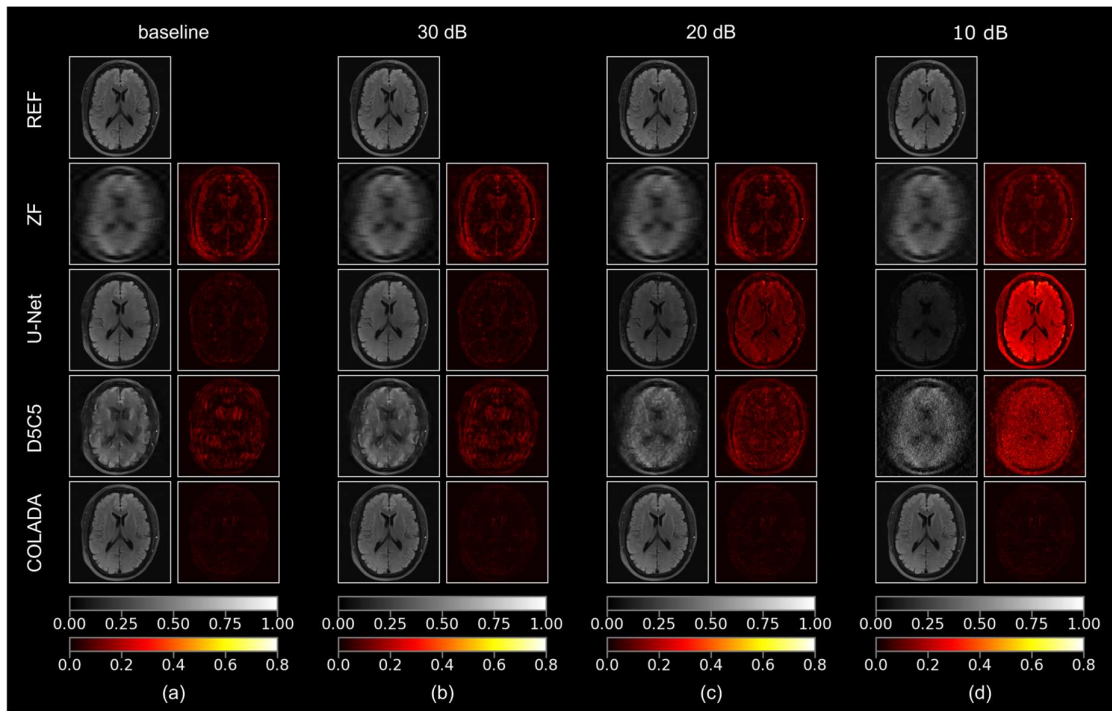


Fig. 8 Qualitative reconstruction comparison of random undersampling in k-space at an acceleration factor of 8X on MR data with AWGN injected to k-space. The reconstructions of a FLAIR scan along with the absolute error are shown for noise levels (a) baseline (no noise injected) (b) 30 dB (c) 20 dB, and (d) 10 dB. ZF: zero-filled input image to DL network reconstructed from undersampled k-space; REF: ground truth fully sampled image; U-Net: reconstructed image using image-to-image mapping DL network. D5C5: reconstructed image using cascaded DL network with data consistency by originally sampled k-space. COLADA: reconstructed image using the COLADA framework. Visual inspection suggests the capability of the COLADA method to suppress noise in the contrastive latent space resulting in reconstructions with minimum noise.

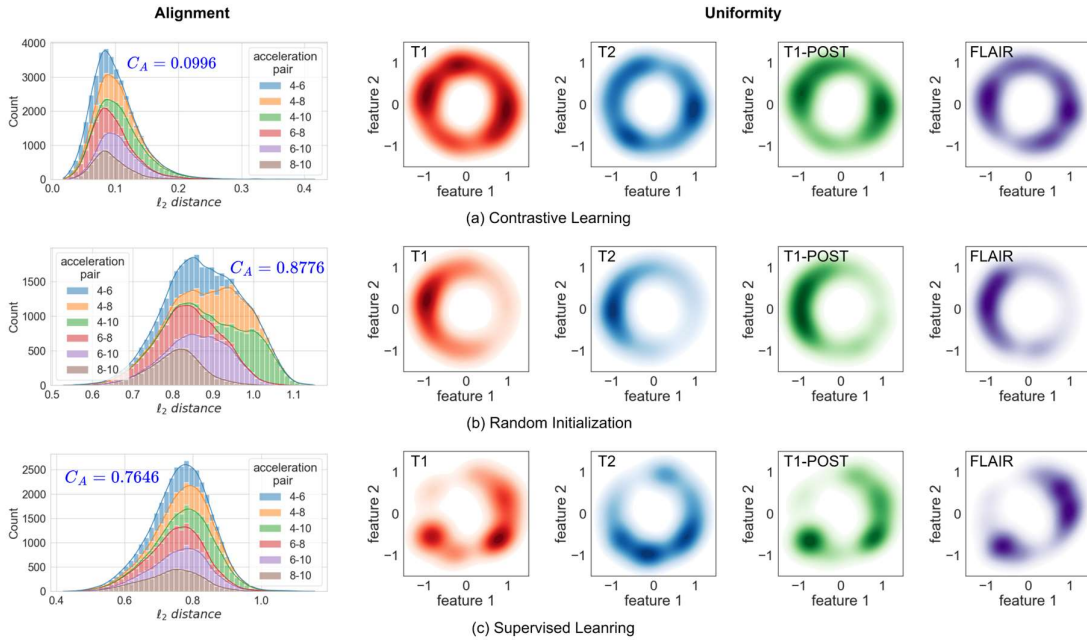


Fig. 9 Analysis of Alignment (left column) and Uniformity (remainder columns) in hypersphere using (a) contrastive learning, (b) random initialization, and (c) supervised learning on the validation dataset. Alignment: Histogram plots demonstrate the histograms of ℓ_2 distances between features of positive pairs visualized between different pairs of acceleration factors. Note that the count between a particular pair of acceleration factors corresponds to the height of the relevant color bar only and should not be mistaken for the height from the zero level. Observe the low ℓ_2 distances in contrastive learning features (the C_A value is given in blue) which indicates the pulling of positive pairs together. Uniformity: KDE plots on the unit circle demonstrate the distributions of two-dimensional features extracted from the encoder visualized separately on the four imaging contrasts, T1, T2, T1-POST, and FLAIR. Observe how contrastive learning distributes features uniformly on the latent space compared to random initialization and supervised learning.

Appendix

A.1 Model Convergence

As explained in Section 3.3, the overall framework consists of two steps. i.e., the contrastive learning and the reconstruction. In our implementation, we train the respective deep learning models in each step for 100 epochs and Fig. A.1 demonstrates the variation of loss on the training and validation sets. Here Fig. A.1(a) shows the infoNCE loss whereas Fig. A.1(b) shows an ℓ_1 -norm loss and it is clear that both losses converge smoothly over epochs.

A.2 Qualitative Reconstruction Performance

The fastMRI brain dataset contains scans belonging to four contrasts and in Fig. 3 we demonstrated two examples of T1 and FLAIR reconstructions. In Fig. A.2 we demonstrate two more examples belonging to T2 and T1-POST reconstructions. Visual inspection showed COLADA achieves high reconstruction quality even at very higher acceleration factors.

A.3 Quantitative Reconstruction Performance

Fig. 4 demonstrated the quantitative boxplot scores for the validation dataset with respect to NMSE, PSNR, and SSIM. The corresponding numerical scores are displayed in Table A.1 in terms of mean and standard deviation for readers' convenience.

A.4 Quantitative Reconstruction Performance on locally acquired data

In Fig. 7, we demonstrated two test cases of T1-weighted image reconstructions from a locally acquired dataset. The corresponding numerical scores are displayed for the validation dataset in Table A.2 in terms of mean and standard deviation.

Table A.1. Quantitative reconstruction comparison of random undersampling in k-space at acceleration factors of 4X, 10X, and 16X with respect to NMSE, PSNR, and SSIM for the four image contrasts (T1, T2, T1POST, and FLAIR) in the validation set. U-Net: reconstructed image using image-to-image mapping DL network. D5C5: reconstructed image using cascaded DL network with data consistency by originally sampled k-space. COLADA: reconstructed image using the COLADA framework. Quantitative scores demonstrate superior reconstruction performance of the COLADA framework.

Contrast	Acceleration Factor	Method	NMSE↓	PSNR↑	SSIM↑
T1	4X	U-Net	0.0117 ± 0.0084	36.54 ± 2.41	0.9340 ± 0.0302
		D5C5	0.0079 ± 0.0031	38.01 ± 3.22	0.9377 ± 0.0326
		COLADA	0.0050 ± 0.0018	39.98 ± 3.28	0.9512 ± 0.0283
	10X	U-Net	0.0253 ± 0.0156	33.13 ± 2.84	0.8985 ± 0.0474
		D5C5	0.0374 ± 0.0172	31.28 ± 3.12	0.8717 ± 0.0587
		COLADA	0.0142 ± 0.0055	35.44 ± 3.49	0.9166 ± 0.0464
	16X	U-Net	0.1090 ± 0.0687	27.15 ± 2.86	0.8288 ± 0.0485
		D5C5	0.0772 ± 0.0335	28.13 ± 2.95	0.8247 ± 0.0606
		COLADA	0.0370 ± 0.0205	31.50 ± 3.44	0.8810 ± 0.0528
T2	4X	U-Net	0.0142 ± 0.0019	33.04 ± 1.19	0.9284 ± 0.0110
		D5C5	0.0089 ± 0.0016	35.09 ± 1.43	0.9382 ± 0.0110
		COLADA	0.0053 ± 0.0010	37.40 ± 1.53	0.9562 ± 0.0086
	10X	U-Net	0.0409 ± 0.0076	28.48 ± 1.51	0.8702 ± 0.0212
		D5C5	0.0573 ± 0.0159	27.12 ± 1.73	0.8371 ± 0.0320
		COLADA	0.0211 ± 0.0056	31.42 ± 1.60	0.9065 ± 0.0191
	16X	U-Net	0.1253 ± 0.0320	23.69 ± 1.70	0.7684 ± 0.0363
		D5C5	0.1176 ± 0.0304	23.97 ± 1.83	0.7594 ± 0.0427
		COLADA	0.0568 ± 0.0214	27.28 ± 2.26	0.8496 ± 0.0339
T1-POST	4X	U-Net	0.0073 ± 0.0022	37.08 ± 1.18	0.9506 ± 0.0080
		D5C5	0.0053 ± 0.0018	38.49 ± 1.45	0.9524 ± 0.0088
		COLADA	0.0032 ± 0.0010	40.61 ± 1.28	0.9656 ± 0.0060
	10X	U-Net	0.0177 ± 0.0059	33.24 ± 1.51	0.9200 ± 0.0145
		D5C5	0.0275 ± 0.0090	31.33 ± 1.90	0.8926 ± 0.0240
		COLADA	0.0095 ± 0.0036	35.99 ± 1.52	0.9382 ± 0.0123
	16X	U-Net	0.0991 ± 0.0558	26.23 ± 3.15	0.8410 ± 0.0483
		D5C5	0.0723 ± 0.0286	27.28 ± 2.51	0.8361 ± 0.0426
		COLADA	0.0334 ± 0.0194	30.96 ± 3.14	0.8962 ± 0.0343
FLAIR	4X	U-Net	0.0101 ± 0.0024	35.89 ± 1.75	0.9236 ± 0.0196
		D5C5	0.0082 ± 0.0024	36.84 ± 1.96	0.9298 ± 0.0190
		COLADA	0.0049 ± 0.0011	39.05 ± 2.04	0.9467 ± 0.0171
	10X	U-Net	0.0255 ± 0.0077	31.96 ± 1.81	0.8758 ± 0.0251
		D5C5	0.0460 ± 0.0187	29.54 ± 1.74	0.8367 ± 0.0321
		COLADA	0.0158 ± 0.0054	34.08 ± 1.89	0.9006 ± 0.0234
	16X	U-Net	0.0616 ± 0.0153	28.07 ± 2.01	0.8152 ± 0.0334
		D5C5	0.0739 ± 0.0247	27.38 ± 1.66	0.7911 ± 0.0344
		COLADA	0.0346 ± 0.0125	30.71 ± 1.98	0.8600 ± 0.0274

Table A.2. Quantitative reconstruction scores of COLADA of random undersampling in k-space at acceleration factors of 4X, 6X, 8X, and 10X with respect to NMSE, PSNR, and SSIM for the validation set of the locally acquired T1-weighted data.

Acceleration Factor	NMSE↓	PSNR↑	SSIM↑
4X	0.0019 ± 0.0005	40.43 ± 1.50	0.9706 ± 0.0048
6X	0.0036 ± 0.0011	37.59 ± 1.40	0.9594 ± 0.0063
8X	0.0052 ± 0.0015	36.00 ± 1.35	0.9498 ± 0.0084
10X	0.0071 ± 0.0022	34.73 ± 1.51	0.9409 ± 0.0107

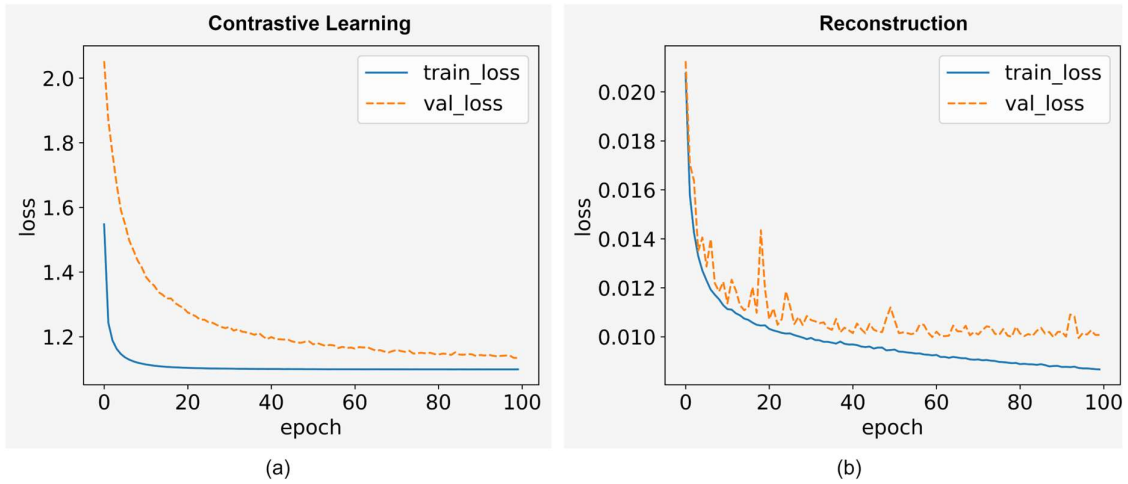


Fig. A.1 Training and validation curves of (a) Contrastive Learning (infoNCE loss) and (b) Reconstruction (ℓ_1 -norm loss). Observe the smooth convergence in both cases.

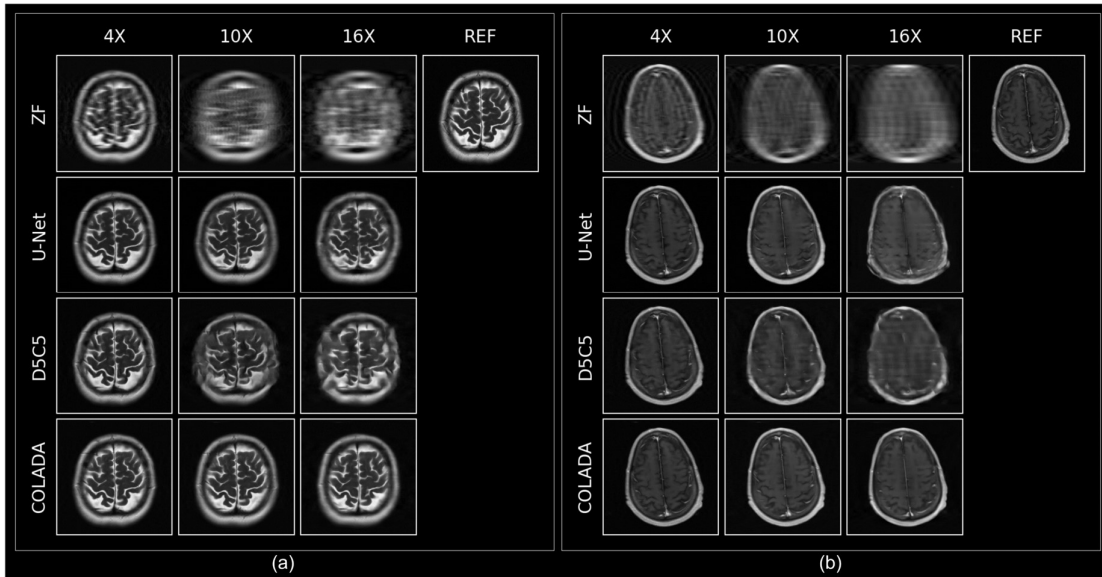


Fig. A.2 Qualitative reconstruction comparison of random undersampling in k-space at acceleration factors of 4X, 10X, and 16X for two different contrasts, (a) T2 and (b) T1-POST. ZF: zero-filled input image to DL network reconstructed from undersampled k-space; REF: ground truth fully sampled image; U-Net: reconstructed image using image-to-image mapping DL network. D5C5: reconstructed image using cascaded DL network with data consistency by originally sampled k-space. COLADA: reconstructed image using the COLADA framework. Visual inspection suggests superior reconstruction quality of COLADA even at high acceleration factors.